J. Fluid Mech. (2013), *vol.* 735, *pp.* 473–498. © Cambridge University Press 2013
doi:10.1017/jfm.2013.510

Wall effects on self-diffusiophoretic Janus particles: a theoretical study

Darren G. Crowdy†

Department of Mathematics, Imperial College London, 180 Queen's Gate, London SW7 2AZ, UK

(Received 13 May 2013; revised 16 August 2013; accepted 21 September 2013;
first published online 24 October 2013)

We present a theoretical investigation of the self-diffusiophoresis of a class of two-faced, two-dimensional Janus particles propelled by the production of gradients in the concentration of a solute diffusing into a surrounding fluid at zero Reynolds and Péclet numbers. Those concentration gradients produce a tangential boundary slip resulting in translation and rotation of the particle, as a consequence of the fact that it is free of both force and torque. The model Janus particles studied here have piecewise constant surface mobilities and surface activities over two faces. An isolated circular Janus particle is studied first and its speed of locomotion in free space is found analytically. Confinement effects are then investigated by placing such a Janus particle near a straight no-slip wall. The governing nonlinear dynamical system is found in explicit form. It is used to study how the geometry, location and orientation of the particle relative to the wall affect its motion. It is found that if the particles do not hit the wall in finite time they are eventually repelled away from it.

Key words: low-Reynolds-number flows, Janus particle

1. Introduction

An important technological challenge, for drug-delivery systems and in micromechanics, is to develop ways to enable small-scale objects to perform autonomous controlled motion. A promising route for producing such artificial microswimmers, or 'nanomotors', is to endow a particle of fixed shape with anisotropically patterned physico-chemical properties (Anderson 1989; Paxton *et al.* 2004). Among the many examples are so-called Janus colloids, which are chemically reactive beads or rods consisting of one of more portions of their boundaries, or 'faces', having different chemical, electrical or thermomechanical properties (Paxton *et al.* 2004; Golestanian, Liverpool & Ajdari 2007; Ebbens & Howse 2010). These particles take advantage of self-phoretic effects where gradients of solute concentration, electric or temperature fields interact with the particle's surface properties to create slip velocities that lead to net propulsion and rotation, by virtue of the constraints that the particle is free of any net force or torque. Recently evidence has been given (Michelin *et al.* 2013) that chemical anisotropy of a colloidal particle is not necessary for locomotion but that an interplay between surface osmotic flows and solute advection is also enough. Other propulsion mechanisms exploit Marangoni effects at the surface to induce locomotion (Thutupalli, Seemann & Herminghaus

† Email address for correspondence: d.crowdy@imperial.ac.uk

https://doi.org/10.1017/jfm.2013.510 Published online by Cambridge University Press

2011). Lauga & Davis (2012) have studied the phenomenon of viscous Marangoni self-propulsion by considering a model 'boat', on the surface of a viscous fluid, which is Janus-like in having one portion of its boundary providing the driving mechanism via an imposed surfactant distribution with the rest of its boundary exhibiting a different Neumann-type boundary condition.

This paper focuses on the dynamics of catalytic nanomotor devices (Anderson 1989; Paxton *et al.* 2004) where it is anistropy of the surface patterning that leads to particle motion. The recent review of Golestanian *et al.* (2007) describes the theoretical considerations relevant to the design of such self-propelling particles. The basic idea is that a particle has an asymmetric distribution of catalyst on its surface; the associated chemical reactions produce an asymmetric distribution of reactants that leads to propulsion. This process whereby chemicals or solute diffuse into the ambient fluid to give rise to the phoretic surface slip velocities is called 'self-diffusiophoresis' because the diffusive driving mechanism is self-generated and is not due to any external fields. Here we document a theoretical investigation into how such self-diffusiophoretic particles move near a no-slip, chemically inactive wall.

Our study of wall effects, which takes place within a two-dimensional model formulation, follows in the spirit of the related two-dimensional studies of electrophoresis near a wall due to Keh, Horng & Kuo (1991) and Zhao & Bau (2007). In those electrophoretic systems, which are driven by external electric fields, confining walls are found to have a dramatic effect on the particle dynamics. While the work of Zhao & Bau (2007) indicates that symmetric polarizable particles are repelled from insulating walls, experiments involving metallo-dielectric Janus particles performed by Gangwal *et al.* (2008) show a tendency for those more exotic particles to be attracted to the surface, eventually moving parallel to the wall within a particle diameter from it. Kilic & Bazant (2011) rationalize this unexpected behaviour and attribute it to a hydrodynamic torque which serves to rotate the forward facing (dielectric) side, or 'nose', of a spherical Janus particle towards the wall. Under some conditions, the theory predicts a state of steady translation parallel to the wall with an equilibrium tilt angle which is consistent with experimental observations (Gangwal *et al.* 2008). In their study Kilic & Bazant (2011) carry out full numerical simulations of their model system. Further theoretical work on this problem has been contributed recently by Miloh (2013).

Since there are no external fields in the self-diffusiophoresis problem capable of exerting hydrodynamic torques on a particle, there is no reason to expect that the dynamics of self-propelling Janus particles near a wall will share this feature of wall attraction. Very little theoretical work on confinement effects on Janus particle self-diffusiophoresis can be found in the literature, although one theoretical study has been given by Popescu, Dietrich & Oshanin (2009). Those authors used spherical confining geometries and particles driven by a single localized reaction site on the surface to study how the speed of the particle is affected. It is both instructive and useful to complement this existing work with studies of the two-dimensional analogues – which do not apparently appear in the literature – not least because a certain amount can be achieved theoretically and this throws light on qualitative features of the three-dimensional problem. The work of Popescu *et al.* (2009) involves a much more detailed analysis of the physico-chemical mechanisms at work in driving the self-propulsion and, in particular, the extent to which the standard theory of phoresis pertains to such systems. Notwithstanding such important matters, given the complexity of the geometry, here we strip back the complexity of the physical model

https://doi.org/10.1017/jfm.2013.510 Published online by Cambridge University Press

to the simple one described by Golestanian *et al.* (2007) and focus on exploring its consequences.

First we introduce our model Janus particle as an isolated two-faced circular particle which is a zero net source of solute; that solute diffuses around the particle at zero Péclet number with diffusion coefficient D. If the particle is actuated by a ratio r of its surface having uniform surface mobility M_1 and surface activity A_1, with the remainder having mobility M_2, we show that the (reduced) particle speed is

$$\frac{U}{U_0} = -\frac{\sin \pi r}{\pi}\left[\frac{r + \lambda(1-r)}{1-r}\right], \tag{1.1}$$

where

$$U_0 = \frac{A_1 M_1}{D}, \quad \lambda = \frac{M_2}{M_1}. \tag{1.2}$$

This single-particle velocity is already an interesting nonlinear function of the coverage ratio r with linear dependence on the ratio of surface mobilities λ. The ramifications of this formula are explored in detail in § 2.

The analysis of § 2 illustrates, in a simple context, the mathematical ideas to be employed in the more complicated scenario of § 3 when the same Janus particle is placed in the half-space near a confining straight wall. The fluid region between the wall and the particle is doubly connected and requires appropriate modification of the analysis. Our approach is to extend and adapt earlier work by the author (Crowdy 2011) where a conformal mapping method is combined with the reciprocal theorem for Stokes flow and a known exact solution for the so-called 'dragging problem' for a cylinder near a no-slip wall to find the required linear and angular velocities of the Janus particle. It turns out that the latter can be found in explicit form.

2. An isolated Janus particle

Consider an isolated circular Janus particle instantaneously centred at the origin and having unit radius. We follow the theoretical formulation laid out in the review by Golestanian *et al.* (2007). Let the solute concentration exterior to the particle be denoted by $c(x, y)$. In the zero Péclet number limit the boundary value problem for $c(x, y)$ is to solve Laplace's equation

$$\nabla^2 c = 0 \tag{2.1}$$

outside the particle with the Neumann boundary condition

$$-D\boldsymbol{n} \cdot \nabla c = A, \tag{2.2}$$

where D is the diffusion coefficient and A is the local surface activity. Positive values of surface activity A correspond to solute emitting surfaces. We assume that there is no solute in the far field. The particle is situated in fluid of viscosity μ assumed to be in the zero Reynolds number regime. Once the solute concentration has been found from the above boundary value problem, the local phoretic slip velocity $\boldsymbol{u}_s$ on the boundary is

$$\boldsymbol{u}_s = M(\boldsymbol{I} - \boldsymbol{nn}) \cdot \nabla c, \tag{2.3}$$

where M is the surface mobility, and it is this surface velocity that will drive a local Stokes flow around the particle.

https://doi.org/10.1017/jfm.2013.510 Published online by Cambridge University Press

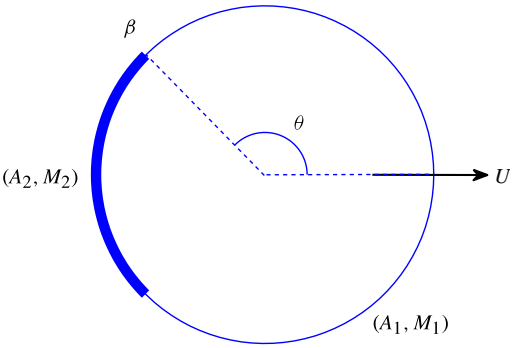


FIGURE 1. (Colour online) An isolated circular Janus particle of unit radius with C_1 occupying $r = \theta/\pi$ of the surface and C_2 (the thick line portion) occupying the remainder. Its locomotion speed is given in (1.1) as a function of r and surface mobility ratio λ.

Our interest is in the study of two-faced Janus particles and it is necessary to specify their type. Following Golestanian *et al.* (2007) we make the special choice of piecewise constant surface activity A and mobility M given by

$$(A, M) = \begin{cases} (A_1, M_1) & \text{on } C_1, \\ (A_2, M_2) & \text{on } C_2, \end{cases} \tag{2.4}$$

where A_i, M_i for $i = 1, 2$ are constants; the portion of the boundary with $\arg[z] \in [-\theta, \theta]$ is denoted by C_1 while the remainder of the boundary is C_2 as shown in figure 1. These are the two 'faces' of the particle. An advantage of the piecewise constant choice (2.4) is that it requires only a choice of the constants rather than a full spatial specification of the functional profiles for the surface activity and mobility, for which more detailed modelling of the surface reactions would really be needed. On the other hand, there is a mathematical disadvantage because the discontinuous data can lead to subtleties in dealing effectively with the induced singularities in the field quantities at those points of discontinuity. The latter complication is overcome here by explicit resolution of those boundary point singularities. This is important because these singularities are the principal determinant of the particle dynamics.

It is convenient to write the corresponding boundary conditions for $c(x, y)$ as

$$\frac{\partial c}{\partial n} = \begin{cases} a & \text{on } C_1, \\ b & \text{on } C_2, \end{cases} \tag{2.5}$$

where $a = -A_1/D$ and $b = -A_2/D$. An assumption made throughout our work – mainly to reduce the size of the parameter space but also because the same assumption has been made in prior studies (Golestanian *et al.* 2007) – is to insist that the particle is not a net source of solute. This means that a and b are not independent but are related by

$$2a\theta + b(2\pi - 2\theta) = 0 \quad \text{or} \quad \frac{b-a}{\pi} = \frac{a}{\theta - \pi}. \tag{2.6}$$

This assumption can be relaxed, but that case is not considered here.

https://doi.org/10.1017/jfm.2013.510 Published online by Cambridge University Press

2.1. *Complex variable formulation*

Let the two points on the boundary at which the boundary conditions change be $\beta = \mathrm{e}^{\mathrm{i}\theta}$ and $\overline{\beta}$ as shown in figure 1. Since the solute concentration is harmonic outside the particle we can introduce the complex analytic function $w(z)$, with $z = x + \mathrm{i}y$, such that

$$c(x, y) = \mathrm{Re}[w(z)]. \tag{2.7}$$

The boundary condition (2.5) can be written in complex form as

$$\mathrm{Re}\left[\frac{\mathrm{d}w}{\mathrm{d}z} z\right] = \begin{cases} a & \text{on } C_1, \\ b & \text{on } C_2. \end{cases} \tag{2.8}$$

By virtue of the condition that there is no solute in the far field, together with the constraint that the Janus particle is not a source of solute, then

$$w(z) \sim O(1/z) + \cdots, \quad \frac{\mathrm{d}w}{\mathrm{d}z} \sim O(1/z^2) \quad \text{as } z \to \infty. \tag{2.9}$$

The function $z\mathrm{d}w/\mathrm{d}z$ is therefore analytic and single-valued outside the particle. Let

$$\eta(z) = \mathscr{A}\left(\frac{z-\beta}{z-\overline{\beta}}\right), \quad \mathscr{A} = \mathrm{e}^{\mathrm{i}(\pi-\theta)}. \tag{2.10}$$

This is the Möbius map to a complex η-plane that sends C_1 to the positive real η-axis and C_2 to the negative real η-axis. (There is a minor abuse of notation, here and elsewhere, in that η is taken to mean both the mapping function and the coordinate in the transformed plane, but it should be clear from the context which is meant.) If we now define

$$z\frac{\mathrm{d}w}{\mathrm{d}z} = a - \frac{\mathrm{i}(b-a)}{\pi} \log \eta(z), \tag{2.11}$$

where we choose the branch of the logarithm so that

$$\mathrm{Im}[\log \eta(z)] = \begin{cases} 0 & \text{on } C_1, \\ \pi & \text{on } C_2, \end{cases} \tag{2.12}$$

then it can be verified that (2.11) satisfies (2.8) as well as the far-field condition (2.9), provided a and b satisfy (2.6). Equation (2.11) therefore gives the required solute concentration in the bulk since

$$w(z) = \int^z \left[\frac{a}{z'} - \frac{\mathrm{i}(b-a)}{\pi} \frac{\log \eta(z')}{z'}\right] \mathrm{d}z'. \tag{2.13}$$

It is not necessary to evaluate this indefinite integral because only (2.11) is needed for present purposes. From (2.3) the (complex) phoretic slip velocity on the boundary is

$$u_s = \begin{cases} M_1 \mathrm{Re}\left[\left(\dfrac{\mathrm{d}w}{\mathrm{d}z}\right)(\mathrm{i}z)\right] \mathrm{i}z & \text{on } C_1, \\ M_2 \mathrm{Re}\left[\left(\dfrac{\mathrm{d}w}{\mathrm{d}z}\right)(\mathrm{i}z)\right] \mathrm{i}z & \text{on } C_2. \end{cases} \tag{2.14}$$

https://doi.org/10.1017/jfm.2013.510 Published online by Cambridge University Press

Hence, from the solution (2.11), we deduce that

$$u_s = \begin{cases} \dfrac{M_1(b-a)}{\pi} \mathrm{i}z \log|\eta(z)| & \text{on } C_1, \\ \dfrac{M_2(b-a)}{\pi} \mathrm{i}z \log|\eta(z)| & \text{on } C_2. \end{cases} \tag{2.15}$$

It is now usual (Golestanian *et al.* 2007) to invoke the reciprocal theorem of Stokes flow to produce an integral formula for the swimmer speed based on knowledge of the solution to the associated 'dragging problem' (indeed, this is precisely what will be done in § 3 when we introduce a solid wall). However, for an isolated two-dimensional swimmer the well-known Stokes paradox precludes use of the reciprocal theorem since the solution to the dragging problem does not exist. Nevertheless, the required (complex) particle speed is still given by the simple integral

$$U = -\frac{1}{2\pi} \int_0^{2\pi} u_s \, \mathrm{d}\phi, \tag{2.16}$$

where $z = \mathrm{e}^{\mathrm{i}\phi}$ – a convenient fact discussed, for example, by Squires & Bazant (2006). We therefore determine that

$$U = -\frac{M_1(b-a)}{2\pi^2} \int_{C_1} \log|\eta(z)| \, \mathrm{d}z - \frac{M_2(b-a)}{2\pi^2} \int_{C_2} \log|\eta(z)| \, \mathrm{d}z. \tag{2.17}$$

Now arises the mathematical point alluded to earlier: these integrals are improper because the integrand has two logarithmic singularities at the edges of the integration contours. While suitable numerical integration schemes can be used it is advisable to transfer these integrals to the complex η-plane where the methods of complex analysis lead to their closed-form evaluation. Indeed,

$$U = -\frac{M_1(b-a)}{2\pi^2} \int_{\infty}^{0} \log|\eta| P(\eta) \, \mathrm{d}\eta - \frac{M_2(b-a)}{2\pi^2} \int_{0}^{-\infty} \log|\eta| P(\eta) \, \mathrm{d}\eta, \tag{2.18}$$

where

$$P(\eta) = \frac{\mathscr{A}(\beta - \overline{\beta})}{(\eta - \mathscr{A})^2} \tag{2.19}$$

is a rational function with a pole at $\eta = \mathscr{A}$. The integral in (2.18) can be computed analytically using the results from residue calculus summarized in appendix B. With $\beta = \mathrm{e}^{\mathrm{i}\theta}$ we find

$$U = \frac{a \sin\theta [M_1\theta + M_2(\pi - \theta)]}{\pi(\pi - \theta)}, \tag{2.20}$$

where we have made use of (2.6) to eliminate b in favour of a together with the fact that $\arg[\mathscr{A}] = \pi - \theta$. With the coverage ratio defined by $r = \theta/\pi$, equation (2.20) is the result given in (1.1) and (1.2).

In the limit $\theta \to 0$, then $U \to 0$ since, for fixed a, the value of $b \to 0$ and the actuation mechanism for the particle motion vanishes. On the other hand, as $\theta \to \pi$,

$$U \to -\frac{A_1 M_1}{D}, \tag{2.21}$$

corresponding to a localized reaction site on the boundary (cf. Golestanian, Liverpool & Ajdari 2005; Popescu *et al.* 2009).

https://doi.org/10.1017/jfm.2013.510 Published online by Cambridge University Press

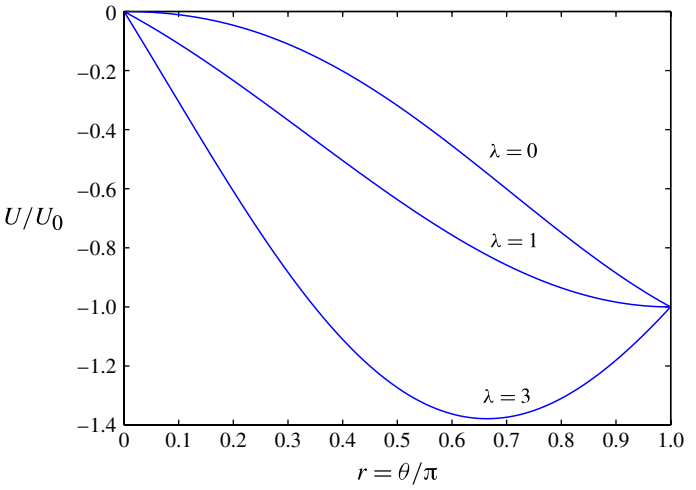


FIGURE 2. (Colour online) Reduced particle speed U/U_0 against coverage ratio r for a single isolated particle with varying ratio of surface mobilities $\lambda = 0, 1, 3$. The graph is monotonic decreasing for $\lambda \in (0, 1)$, but there exists a local minimum for any $\lambda > 1$ (e.g. for $\lambda = 3$). Hence for $\lambda > 1$ there is an optimal geometrical arrangement of the two faces that maximizes the particle velocity.

The particle speed (1.1) is found to be monotonic decreasing as a function of r for $\lambda \in (0, 1)$ but it has a local minimum for any $\lambda > 1$. This means that for $\lambda > 1$ there is an optimal geometrical configuration of the two faces that maximizes the particle velocity. The critical coverage ratio r_* at these stationary points is given by a solution of the nonlinear equation

$$(r_* - 1)[1 + (1 - \lambda)(r_* - 1)] - \frac{\tan(\pi r_*)}{\pi} = 0. \tag{2.22}$$

Figure 3 shows a graph of r_* as a function of λ. Golestanian *et al.* (2007) report on the swimming speed for the analogous two-faced spherical Janus particle when the two faces occupy two equal hemispheres – corresponding to $r = 1/2$ here – with the result, rewritten in present notation,

$$U = \frac{1}{8D}(A_2 - A_1)(M_1 + M_2). \tag{2.23}$$

However those authors do not give the result for two-faced particles with general coverage ratio. Instead, presumably motivated by designs for Janus particles realizable by available fabrication techniques, they break symmetry by investigating a so-called 'Saturn' particle having three 'slices', or bands, of different surface activities and mobilities. For such particles they identify a similar phenomenon to that reported above, namely, the existence of an optimal geometrical configuration (in their case, for the size of a central equatorial belt region between two polar caps) for which the particle speed is maximized for a particular range of surface mobility ratios. Our analysis, summarized in figure 2, shows that the same phenomenon is observable for the geometrically simpler two-faced Janus particles when $\lambda > 1$. As $\lambda \to \infty$ the optimal configuration for maximum speed is to have the two faces occupy exactly half the particle surface (i.e., $r_* \to 1/2$).

https://doi.org/10.1017/jfm.2013.510 Published online by Cambridge University Press

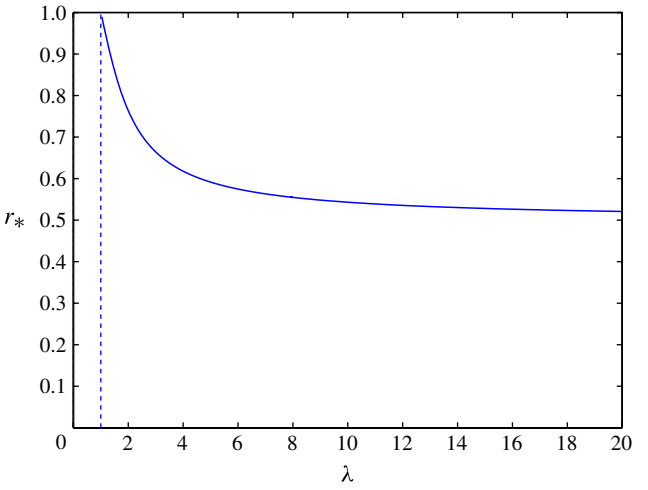


FIGURE 3. (Colour online) Graph of coverage ratio r_* corresponding to the maximum particle speed for an isolated Janus particle. For $\lambda \in (0, 1)$ there is no solution for r_*. As $\lambda \to \infty$, $r_* \to 1/2$ so the particle with the highest speed corresponds to the two faces occupying equal halves of the particle surface.

A final observation which will be useful later is to note that for $\lambda = 1$, so that the surface mobilities of the two faces are equal, the particle moves to the left (i.e., towards negative x values) when $A_1 > 0$, i.e., the particle moves in the direction of C_2, the solute-absorbing face of the particle.

3. Janus particle near a wall

Now that the free-space motion of the Janus particle of interest has been determined, we ask how that particle evolves if it is confined to the upper half-plane above a straight wall along the x-axis. To proceed we first set up an auxiliary complex ζ-plane associated with a conformal mapping that will facilitate our analysis. Although neither the boundary value problem for the solute concentration nor that determining the Stokes streamfunction are conformally invariant, there is still considerable advantage in adopting a conformal mapping approach for the analysis.

3.1. *Conformal mapping*

Suppose the Janus particle has radius s and is centred instantaneously at $(0, d)$ for $d > s$. The fluid region above the wall and exterior to the Janus particle is a doubly connected region and a conformal mapping to it from a parametric annulus $\rho < |\zeta| < 1$ is the Möbius map

$$z(\zeta) = \mathrm{i}R\left(\frac{\zeta + 1}{\zeta - 1}\right), \tag{3.1}$$

where

$$\rho = \frac{d}{s} - \sqrt{\left(\frac{d}{s}\right)^2 - 1}, \quad R = d\left(\frac{\rho^2 - 1}{\rho^2 + 1}\right). \tag{3.2}$$

https://doi.org/10.1017/jfm.2013.510 Published online by Cambridge University Press

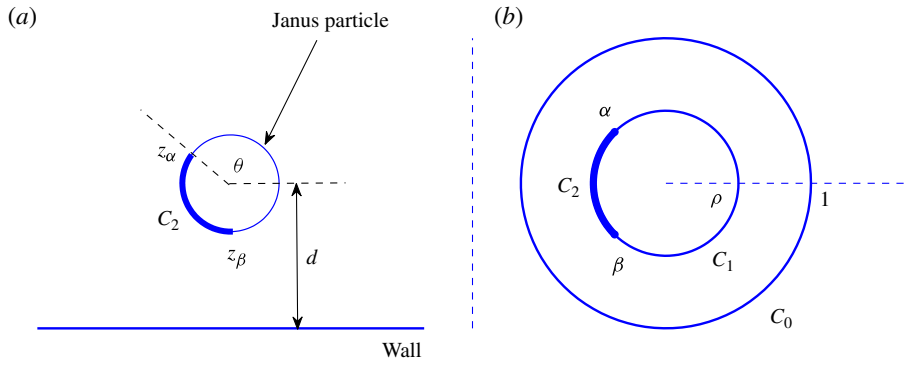


FIGURE 4. (Colour online) (*a*) A two-faced cylindrical Janus particle of radius s situated with its centre at distance d above an infinite straight wall. (*b*) The preimage annulus $\rho < |\zeta| < 1$ with $|\zeta| = 1$ mapping to the real z-axis and $|\zeta| = \rho$ mapping to the Janus particle under the Möbius map (3.1).

This conformal mapping is one used previously by the author (Crowdy 2011). The unit circle, denoted by C_0, maps to the wall and $|\zeta| = \rho$ maps to the boundary of the particle. Let z_α and z_β be the two points on the particle boundary where

$$z_\alpha = \mathrm{i}d + s\mathrm{e}^{\mathrm{i}\theta}, \quad z_\beta = \mathrm{i}d + s\mathrm{e}^{\mathrm{i}(\theta+\chi)}. \tag{3.3}$$

These two points mark the boundaries of the two faces of the Janus particle. The parameter $\chi > 0$ is some fixed real parameter reflecting the amount of the particle surface occupied by face C_2. The preimages of z_α and z_β in the ζ-plane are denoted by α and β and, considered in either plane of reference, we will continue to refer to the two boundary portions as C_1 and C_2. The parameter θ is the instantaneous tilt angle of the point z_α relative to the x-axis (or the wall). The linear and angular velocity of the particle will be denoted

$$\boldsymbol{U}' = (U, V, 0), \quad \boldsymbol{\Omega}' = (0, 0, \Omega). \tag{3.4}$$

The objective is to determine $\boldsymbol{U}'$ and $\boldsymbol{\Omega}'$.

3.2. *Reciprocal theorem*

To find $\boldsymbol{U}'$ and $\boldsymbol{\Omega}'$ we invoke ideas originally developed by the author (Crowdy 2011) for circular 'treadmilling' swimmers near a no-slip wall where the actuation is different to the diffusiophoretic one considered here. The main idea of that paper is to show that the reciprocal theorem of Stokes flow, together with knowledge of an exact solution of the 'dragging problem' for a cylinder near a no-slip wall, can be combined to deduce explicit integral expressions for the particle velocities. Our purpose here is to show that the same mathematical machinery can be used to produce an explicit form for the dynamical system governing the motion of the self-diffusiophoretic Janus swimmer near a wall.

The reciprocal theorem (Crowdy 2011) implies that

$$\boldsymbol{F}\cdot\boldsymbol{U}' + \boldsymbol{\Omega}'\cdot\boldsymbol{T} = -\oint_{|z-z_d|=s} \boldsymbol{U}_{si}\sigma_{ij}n_j \,\mathrm{d}s, \tag{3.5}$$

where $\boldsymbol{F} = (F_x, F_y, 0)$ and $\boldsymbol{T} = (0, 0, T)$ are the force and torque on the cylinder in the 'dragging problem', z_d is the location of the particle centre, σ_{ij} is the associated

https://doi.org/10.1017/jfm.2013.510 Published online by Cambridge University Press

fluid stress tensor, and the vectors $\boldsymbol{U}'$ and $\boldsymbol{\Omega}'$ are the velocities of the particle that we seek. The quantities $\boldsymbol{F}, \boldsymbol{T}$ and σ_{ij} can be found from the known analytic solution to the dragging problem. The latter problem was solved by Jeffrey & Onishi (1981) using bipolar coordinates. Here, however, we follow Crowdy (2011) and perform the analysis in an annulus $\rho < |\zeta| < 1$ in the preimage ζ-plane just introduced. In terms of the ζ variable it can be shown (Crowdy 2011) that

$$-\oint_{|z-z_d|=s} \boldsymbol{U}_{si}\sigma_{ij}n_j \,\mathrm{d}s = -\mathrm{Re}\left[2\mu\mathrm{i}\oint_{|\zeta|=\rho} \overline{U_s}\frac{\mathrm{d}\mathscr{H}}{\mathrm{d}\zeta}\,\mathrm{d}\zeta\right] \tag{3.6}$$

for an analytic function $\mathrm{d}\mathscr{H}/\mathrm{d}\zeta$, which takes various rational function forms corresponding to different solutions of the dragging problem.

3.3. *The solute concentration*

The analysis to determine the solute concentration in the bulk will largely follow the single-particle analysis of § 2, although we now work in the preimage ζ annulus. As before we introduce $w(z)$ such that

$$c(x, y) = \mathrm{Re}[w(z)], \tag{3.7}$$

where $c(x, y)$ is the single-valued harmonic concentration density of the solute in the half-plane above the wall and outside the Janus particle. We assume that the wall is chemically inactive so there is no flux of solute through the wall. The boundary condition there is

$$\frac{\partial c}{\partial n} = 0 \quad \text{on } C_0. \tag{3.8}$$

As before, the boundary conditions on the two faces of the Janus particle C_1 and C_2 are taken to be

$$\frac{\partial c}{\partial n} = \begin{cases} a & \text{on } C_1, \\ b & \text{on } C_2. \end{cases} \tag{3.9}$$

In order that the particle is not a source of solute it is necessary that

$$b\chi + a(2\pi - \chi) = 0 \quad \text{or} \quad (b - a) = -\frac{2\pi a}{\chi}. \tag{3.10}$$

The far-field behaviour of $w(z)$ is then as given in (2.9). In complex form the boundary conditions (3.8) and (3.9) can be written as

$$\mathrm{Re}\left[\frac{\mathrm{d}w}{\mathrm{d}z}(-\mathrm{i})\frac{\mathrm{d}z}{\mathrm{d}s}\right] = \begin{cases} 0 & \text{on } C_0, \\ a & \text{on } C_1, \\ b & \text{on } C_2, \end{cases} \tag{3.11}$$

where we have used the fact that the complex unit normal is $-\mathrm{i}\mathrm{d}z/\mathrm{d}s$ and s denotes the arclength around the boundary in the physical plane. The unit tangents on $|\zeta| = \rho, 1$ are

$$\frac{\mathrm{d}z}{\mathrm{d}s} = -\frac{\mathrm{i}\zeta z'(\zeta)}{|z'(\zeta)|} \quad \text{on } C_0, \qquad \frac{\mathrm{d}z}{\mathrm{d}s} = +\frac{\mathrm{i}\zeta z'(\zeta)}{\rho|z'(\zeta)|} \quad \text{on } C_1, C_2, \tag{3.12}$$

https://doi.org/10.1017/jfm.2013.510 Published online by Cambridge University Press

implying that

$$\mathrm{Re}\left[\frac{\mathrm{d}w}{\mathrm{d}z}\zeta z'(\zeta)\right] = \begin{cases} 0 & \text{on } C_0, \\ \rho a|z'(\zeta)| & \text{on } C_1, \\ \rho b|z'(\zeta)| & \text{on } C_2. \end{cases} \tag{3.13}$$

Now on $|\zeta| = \rho$,

$$|z'(\zeta)| = X(\zeta) \equiv -\frac{2R\zeta}{(\zeta-1)(\rho^2-\zeta)}. \tag{3.14}$$

From the far-field conditions (2.9) the function in square brackets on the left side of (3.13) is seen to be analytic at $\zeta = 1$, but the discontinuity in its boundary data on $|\zeta| = \rho$ will force logarithmic singularities at $\zeta = \alpha$ and β. To account for the latter singularities let

$$G(\zeta) = -X(\zeta)\left[\rho a - \frac{\mathrm{i}\rho(b-a)}{\pi}\log\eta(\zeta)\right], \tag{3.15}$$

where

$$\eta(\zeta) = \mathscr{A}\left[\frac{\zeta-\alpha}{\zeta-\beta}\right], \quad \mathscr{A} = \mathrm{e}^{\mathrm{i}(\pi-\theta)}, \quad \theta = \frac{1}{2}\arg[\beta/\alpha] \tag{3.16}$$

is the Möbius mapping that sends the boundary of the Janus particle to the real η-axis with C_1 mapping to the positive real η-axis and C_2 mapping to the negative real η-axis. The function $X(\zeta)$ is real on the circle $|\zeta| = \rho$ and we choose the branch of the logarithm for which

$$\mathrm{Im}[\log\eta] = \begin{cases} 0 & \text{on } C_1, \\ \pi & \text{on } C_2. \end{cases} \tag{3.17}$$

These facts imply that

$$\mathrm{Re}[G(\zeta)] = \begin{cases} -\rho a X(\zeta) & \text{on } C_1, \\ -\rho b X(\zeta) & \text{on } C_2. \end{cases} \tag{3.18}$$

The addition of $\mathrm{Re}[G(\zeta)]$ to both sides of (3.13) produces

$$\mathrm{Re}\left[\frac{\mathrm{d}w}{\mathrm{d}z}\zeta z'(\zeta) + G(\zeta)\right] = \begin{cases} \mathrm{Re}[G(\zeta)] & \text{on } C_0, \\ 0 & \text{on } C_1, \\ 0 & \text{on } C_2. \end{cases} \tag{3.19}$$

But $G(\zeta)$ has a simple pole at $\zeta = 1$ which we should also handle carefully. Therefore define

$$J(\zeta) = X(\zeta)\left[\rho a - \frac{\mathrm{i}\rho(b-a)}{\pi}\log\eta(1)\right], \tag{3.20}$$

and add its real part to (3.19) to give

$$\mathrm{Re}\left[\frac{\mathrm{d}w}{\mathrm{d}z}\zeta z'(\zeta) + G(\zeta) + J(\zeta)\right] = \begin{cases} \mathrm{Re}[G(\zeta)+J(\zeta)] & \text{on } C_0, \\ \mathrm{Re}[J(\zeta)] & \text{on } C_1, \\ \mathrm{Re}[J(\zeta)] & \text{on } C_2. \end{cases} \tag{3.21}$$

https://doi.org/10.1017/jfm.2013.510 Published online by Cambridge University Press

In fact it can be shown that $\mathrm{Re}[J(\zeta)] = 0$ on $|\zeta| = \rho$, implying the simpler boundary value problem

$$\mathrm{Re}[I(\zeta)] = \begin{cases} \mathrm{Re}[G(\zeta) + J(\zeta)] & \text{on } |\zeta| = 1, \\ 0 & \text{on } |\zeta| = \rho, \end{cases} \tag{3.22}$$

where we define

$$I(\zeta) \equiv \frac{\mathrm{d}w}{\mathrm{d}z}\zeta z'(\zeta) + G(\zeta) + J(\zeta). \tag{3.23}$$

The idea behind these manipulations is to take explicit account of all boundary singularities, and now the form of (3.22) is precisely that of a standard modified Schwarz problem (Crowdy 2008) in the annulus for the single-valued and analytic function $I(\zeta)$ given its real part on the boundary. To solve this we can write

$$I(\zeta) = a_0 + \sum_{n=1}^{\infty} a_n \zeta^n + \sum_{n=1}^{\infty} \frac{a_{-n}\rho^n}{\zeta^n}, \quad \rho < |\zeta| < 1, \tag{3.24}$$

for some set of coefficients $\{a_0, a_n, a_{-n} \,|\, n \geqslant 1\}$ to be found. The data on the right-hand side of (3.21) is smooth and analytic on the boundary circles, so we can represent them as the Fourier series

$$\mathrm{Re}[G(\zeta) + J(\zeta)] = \sum_{n=-\infty}^{\infty} d_n \mathrm{e}^{\mathrm{i}n\theta} \quad \text{on } |\zeta| = 1, \tag{3.25}$$

where the coefficients $\{d_n\}$ are readily determined. Substitution of (3.24) into (3.22) gives the coefficients we seek as

$$\mathrm{Re}[a_0] = d_0, \quad a_n = \frac{2d_n}{1-\rho^{2n}}, \quad a_{-n} = -\frac{2\rho^n \overline{d_n}}{1-\rho^{2n}}, \quad n \geqslant 1. \tag{3.26}$$

As in the free-space case, only the quantity

$$\frac{\mathrm{d}w}{\mathrm{d}z}\zeta z'(\zeta) = I(\zeta) - G(\zeta) - J(\zeta) \tag{3.27}$$

is needed to compute the phoretic slip velocity, and this is now known.

3.4. *Phoretic slip velocity*

We assume the mobility of the wall is zero so that it is a no-slip surface (although the formulation is extendible to the case of wall slippage). The complex form of the phoretic slip velocity on C_j for $j = 1, 2$ is

$$U_s = \mu_j \mathrm{Re}\left[\frac{\mathrm{d}w}{\mathrm{d}z}\frac{\mathrm{d}z}{\mathrm{d}s}\right]\frac{\mathrm{d}z}{\mathrm{d}s}, \quad j = 1, 2. \tag{3.28}$$

After some algebra, and use of the solution (3.27), it is found that

$$\overline{U_s} = M_j \mathrm{Re}\left[\frac{\mathrm{i}(\zeta-1)(\zeta-\rho^2)}{2R\zeta}\{I(\zeta) - G(\zeta) - J(\zeta)\}\right]\frac{(1-\zeta)}{(\rho^2-\zeta)}, \quad j = 1, 2. \tag{3.29}$$

It is convenient to separate $\overline{U_s}$ into two parts,

$$\overline{U_s} = \overline{U}_s^{(s)} + \overline{U}_s^{(r)}, \tag{3.30}$$

https://doi.org/10.1017/jfm.2013.510 Published online by Cambridge University Press

where, for $j = 1, 2$,

$$\overline{U}_s^{(s)} = M_j \mathrm{Re}\left[\frac{\mathrm{i}(\zeta-1)(\zeta-\rho^2)}{2R\zeta}\{-G(\zeta)-J(\zeta)\}\right]\frac{(1-\zeta)}{(\rho^2-\zeta)}, \tag{3.31a}$$

$$\overline{U}_s^{(r)} = M_j \mathrm{Re}\left[\frac{\mathrm{i}(\zeta-1)(\zeta-\rho^2)}{2R\zeta}\{I(\zeta)\}\right]\frac{(1-\zeta)}{(\rho^2-\zeta)}. \tag{3.31b}$$

The contribution $\overline{U}_s^{(s)}$ has two singularities at $\zeta = \alpha$ and β on $|\zeta| = \rho$; the contribution $\overline{U}_s^{(r)}$ is regular and smooth on $|\zeta| = \rho$.

The parameter space in our problem is large: even for a given Janus particle type its linear and angular velocities depend on its orientation relative to, and distance from, the wall. We therefore restrict attention to a particular class of Janus particles that will be investigated in detail. It is assumed that both faces of the Janus particle have the same surface mobility, i.e.

$$M_2 = M_1 = 1. \tag{3.32}$$

We fix $a = -1$, with b chosen as in (3.10) for a given χ, and this sets the time scale for the particle's motion. The negativity of a means that face C_2 will be a solute-absorbing face and, borrowing the terminology of Kilic & Bazant (2011), will act as the 'nose' of the particle. The parameter χ will be varied, thereby allowing us to investigate how the geometrical asymmetry between the two faces affects the near-wall dynamics.

3.5. *Equations of motion*

The particle speeds can be determined from the reciprocal theorem as described in § 3.2. Indeed on use of (3.30) equation (3.6) becomes

$$\boldsymbol{F}\cdot\boldsymbol{U}' + \boldsymbol{\Omega}'\cdot\boldsymbol{T} = -\mathrm{Re}\left[2\mu\mathrm{i}\oint_{|\zeta|=\rho}\left[\overline{U}_s^{(s)} + \overline{U}_s^{(r)}\right]\frac{\mathrm{d}\mathscr{H}}{\mathrm{d}\zeta}\,\mathrm{d}\zeta\right]. \tag{3.33}$$

We now show that all integrals on the right-hand side of (3.33) that are required to find the particle speeds can be computed in closed form.

First, the improper integrals involving $\overline{U}_s^{(s)}$ can be found using residue calculus involving contour deformation about logarithmic branch cuts, as outlined in appendices A and B. The details are omitted since they are standard exercises in complex analysis (Ablowitz & Fokas 1997), but the calculations are the direct analogue of those carried out in § 2.1 for a single particle. As mentioned there, it is significant that these integrals can be computed in closed form because a purely numerical evaluation of them would require special care owing to the singularities on the integration contour.

Second, the integrals involving $\overline{U}_s^{(r)}$ are smooth and can be found using the following results, which are applicable to any arbitrary smooth velocity profile. Suppose a smooth tangential velocity profile imposed on the boundary of the particle (i.e. on $|\zeta| = \rho$) has the form

$$b_n\zeta^n + \overline{b_n}\frac{\rho^{2n}}{\zeta^n}, \quad n \geqslant 0, \tag{3.34}$$

for some complex coefficient b_n. This quantity is real on $|\zeta| = \rho$, and it is important to note that any smooth imposed tangential velocity field can be represented as an infinite

https://doi.org/10.1017/jfm.2013.510 Published online by Cambridge University Press

sum of such terms: the result is just the Laurent expansion of the velocity profile valid on $|\zeta| = \rho$. On use of the reciprocal theorem (3.5), and computation of the resulting integrals by means of the residue theorem, we find

$$(U', V', \Omega') = \begin{cases} (0, 0, -b_0/s), & n = 0, \\ \left(\rho \mathrm{Re}[b_1], -\dfrac{\rho(1-\rho^2)}{(1+\rho^2)}\mathrm{Im}[b_1], -\dfrac{2\rho^2}{r(1+\rho^2)}\mathrm{Re}[b_1]\right), & n = 1, \\ (0, 0, 0), & n > 1. \end{cases} \quad (3.35)$$

Thus only the two modes with $n = 0$ and 1 of the tangential velocity profile, expressed as a Laurent expansion in ζ, lead to any non-trivial particle velocities U', V' and Ω', with the $n = 0$ term serving only to alter the particle's angular velocity. This remarkable observation means here that only two terms of the Laurent expansion (in powers of ζ) of the tangential velocity profile associated with $\overline{U}_s^{(r)}$ contribute to the particle velocities. From (3.31) it can be seen that this tangential profile depends on the function $I(\zeta)$ whose Laurent expansion on $|\zeta| = \rho$ has just been found explicitly in (3.26). In fact only the coefficients a_1 and a_2 as determined in (3.26) contribute to the particle velocity, and formulae for these can be found without difficulty.

We now make three independent choices for solutions to the dragging problem to find the required particle speeds.

3.6. *Particle velocity parallel to the wall*

To determine U' we choose the solution of the dragging problem in which a cylinder is dragged at unit speed parallel to the wall. This means we set (Crowdy 2011)

$$\frac{\mathrm{d}\mathscr{H}(\zeta)}{\mathrm{d}\zeta} = \frac{2F_d}{(1-\rho^2)}\left(1 + \frac{(1-\rho^2)}{\zeta} - \frac{\rho^2}{\zeta^2}\right), \quad F_d = -\frac{1}{\log\rho^2}. \quad (3.36)$$

The complex force on the cylinder in the dragging problem is

$$(F_x, F_y, 0) = \left(\frac{8\pi\mu}{\log\rho^2}, 0, 0\right). \quad (3.37)$$

The residue calculation of the improper part of the integral, with the special choice (3.32), leads to

$$\oint_{|\zeta|=\rho} \overline{U}_s^{(s)} \frac{\mathrm{d}\mathscr{H}}{\mathrm{d}\zeta}\,\mathrm{d}\zeta = -\left(\frac{4\pi\mathrm{i}aF_d}{\chi}\right)\frac{\rho}{1-\rho^2}\left[(\beta-\alpha)\left(1+\frac{1}{\alpha\beta}\right)\right] \quad (3.38)$$

so that, on use of (3.6), the contribution to U' from the $\overline{U}_s^{(s)}$ component is

$$\frac{a}{\chi}\frac{\rho}{1-\rho^2}\mathrm{Re}\left[(\beta-\alpha)\left(1+\frac{1}{\alpha\beta}\right)\right]. \quad (3.39)$$

From (3.35) the contribution to U' from the $\overline{U}_s^{(r)}$ component is

$$\frac{2a\rho}{\chi(1-\rho^2)}\log\left|\frac{1-\beta}{1-\alpha}\right| - \frac{2\rho^3 a}{\chi(1-\rho^4)}\mathrm{Re}[\beta-\alpha]. \quad (3.40)$$

The value of U' is the sum of (3.39) and (3.40).

https://doi.org/10.1017/jfm.2013.510 Published online by Cambridge University Press

3.7. *Particle velocity normal to the wall*

To determine V' we choose the solution of the dragging problem in which a cylinder is dragged at unit speed normal to the wall. Thus we set (Crowdy 2011)

$$\frac{\mathrm{d}\mathscr{H}(\zeta)}{\mathrm{d}\zeta} = 2F_d\left(\frac{1}{\zeta} - \frac{\rho^2}{(1+\rho^2)\zeta^2} - \frac{1}{1+\rho^2}\right), \tag{3.41}$$

with

$$F_d = -\frac{\mathrm{i}}{2(1-\rho^2)/(1+\rho^2) + \log\rho^2}. \tag{3.42}$$

The force on the cylinder in the dragging problem is

$$(F_x, F_y, 0) = \left(0, \frac{4\pi\mu}{(1-\rho^2)/(1+\rho^2) + \log\rho}, 0\right). \tag{3.43}$$

In this case the residue calculation with the special choice (3.32) gives

$$\oint_{|\zeta|=\rho} \overline{U}_s^{(s)} \frac{\mathrm{d}\mathscr{H}}{\mathrm{d}\zeta}\,\mathrm{d}\zeta = \left(\frac{4\pi\mathrm{i}aF_d}{\chi}\right)\frac{\rho}{1+\rho^2}\left[(\alpha\beta-1)\left(\frac{1}{\alpha}-\frac{1}{\beta}\right) + 4\log\left|\frac{1-\alpha}{1-\beta}\right|\right], \tag{3.44}$$

so, on use of (3.6), the contribution V' from the $\overline{U}_s^{(s)}$ component is

$$\frac{a}{\chi}\frac{\rho}{1+\rho^2}\mathrm{Im}\left[(\alpha\beta-1)\left(\frac{1}{\alpha}-\frac{1}{\beta}\right)\right]. \tag{3.45}$$

From (3.35) the contribution to V' from the $\overline{U}_s^{(r)}$ component is found, after some algebra, to be

$$-\frac{2a}{\chi}\frac{\rho(1-\rho^2)}{(1+\rho^2)}\left[\frac{\rho^2}{(1-\rho^4)}\mathrm{Im}[\beta-\alpha] + \frac{1}{(1-\rho^2)}\arg\left[\frac{1-\overline{\beta}}{1-\overline{\alpha}}\right]\right]. \tag{3.46}$$

The value of V' is the sum of (3.45) and (3.46).

3.8. *Angular velocity of the particle*

To determine Ω' we set (Crowdy 2011)

$$\frac{\mathrm{d}\mathscr{H}(\zeta)}{\mathrm{d}\zeta} = \frac{4R\rho^2}{(1-\rho^2)^3}\left(1-\frac{\rho^2}{\zeta^2}\right) + \frac{2R}{(\zeta-1)^2}, \tag{3.47}$$

which corresponds to a solution to the dragging problem where the cylinder is rotated at unit angular velocity near a wall. The corresponding torque in the dragging problem is

$$(0, 0, T) = \left[0, 0, -4\pi s^2\left(\frac{1+\rho^2}{1-\rho^2}\right)\right]. \tag{3.48}$$

With the special choice (3.32) we find

$$\oint_{|\zeta|=\rho} \overline{U}_s^{(s)} \frac{\mathrm{d}\mathscr{H}}{\mathrm{d}\zeta}\,\mathrm{d}\zeta = -\left(\frac{8\pi\mathrm{i}aR}{\chi}\right)\frac{\rho}{(1-\rho^2)^2} \times\left[\rho^2\log\left(\frac{1-\alpha}{1-\beta}\right) + \log\left(\frac{1-\overline{\alpha}}{1-\overline{\beta}}\right) + \frac{\rho^2}{(1-\rho^2)}(\beta-\alpha)\left(1+\frac{1}{\alpha\beta}\right)\right]. \tag{3.49}$$

https://doi.org/10.1017/jfm.2013.510 Published online by Cambridge University Press

Hence, on use of (3.6), the contribution to Ω' from the $\overline{U}_s^{(s)}$ component is

$$-\frac{2a}{s\chi}\left[\log\left|\frac{1-\alpha}{1-\beta}\right|+\frac{\rho^2}{1-\rho^4}\mathrm{Re}\left[(\beta-\alpha)\left(1+\frac{1}{\alpha\beta}\right)\right]\right]. \tag{3.50}$$

From (3.35) the contribution to Ω' from the $\overline{U}_s^{(r)}$ component is found, after some algebra, to be

$$\frac{4a}{s\chi}\frac{\rho^4}{(1-\rho^4)}\left[\log\left|\frac{1-\beta}{1-\alpha}\right|+\frac{1}{(1+\rho^2)}\mathrm{Re}[\beta-\alpha]\right]. \tag{3.51}$$

The value of Ω' is the sum of (3.50) and (3.51).

3.9. *Governing dynamical system*

The system of nonlinear ordinary differential equations governing the motion of the particle centre $(X(t), Y(t))$ and its orientation $\theta(t)$ is given by

$$\dot{X}=U', \quad \dot{Y}=V', \quad \dot{\theta}=\Omega', \tag{3.52}$$

where the prescription for determining U', V' and Ω' has just been described. A combination of all the foregoing results, and some algebraic simplifications, lead to

$$\frac{\mathrm{d}X}{\mathrm{d}t}=\frac{a\rho}{\chi(1-\rho^2)}\left[\frac{1-\rho^2}{1+\rho^2}\mathrm{Re}[\beta-\alpha]+\mathrm{Re}\left[\frac{1}{\alpha}-\frac{1}{\beta}\right]+2\log\left|\frac{1-\beta}{1-\alpha}\right|\right], \tag{3.53a}$$

$$\frac{\mathrm{d}Y}{\mathrm{d}t}=\frac{a\rho}{\chi(1+\rho^2)}\left[\frac{1-\rho^2}{1+\rho^2}\mathrm{Im}[\beta-\alpha]-\mathrm{Im}\left[\frac{1}{\alpha}-\frac{1}{\beta}\right]+2\arg\left[\frac{1-\beta}{1-\alpha}\right]\right], \tag{3.53b}$$

$$\frac{\mathrm{d}\theta}{\mathrm{d}t}=-\frac{2a\rho^2}{s\chi(1-\rho^4)}\left[\frac{1-\rho^2}{1+\rho^2}\mathrm{Re}[\beta-\alpha]+\mathrm{Re}\left[\frac{1}{\alpha}-\frac{1}{\beta}\right]-\left(\frac{1+\rho^4}{\rho^2}\right)\log\left|\frac{1-\beta}{1-\alpha}\right|\right], \tag{3.53c}$$

where parameters ρ, α and β are given in terms of X, Y and θ by

$$\rho=\frac{Y}{s}-\sqrt{\left(\frac{Y}{s}\right)^2-1}, \quad \alpha=\frac{\rho^2-\mathrm{i}\rho\mathrm{e}^{\mathrm{i}\theta}}{1-\mathrm{i}\rho\mathrm{e}^{\mathrm{i}\theta}}, \quad \beta=\frac{\rho^2-\mathrm{i}\rho\mathrm{e}^{\mathrm{i}(\theta+\chi)}}{1-\mathrm{i}\rho\mathrm{e}^{\mathrm{i}(\theta+\chi)}}. \tag{3.54}$$

This is the governing dynamical system for the Janus particle evolution.

4. Results

Henceforth we drop the primes and refer to the particle velocities as U, V and Ω. The problem has certain symmetries which it is useful to exploit. We introduce the angle ϕ, as illustrated in figure 5, to denote the angle made with the wall by the ray joining the particle centre to the midpoint of the solute-absorbing face C_2. By the left–right symmetry it is enough to consider $\phi \in [-\pi/2, \pi/2]$ and to study what happens as face C_2 points towards $x > 0$ at different angles, as indicated in figure 5. Negative and positive values of ϕ in this range correspond to C_2 facing towards and away from the wall respectively, and always towards $x > 0$. It is also enough to consider $\chi \in (0, \pi]$ because the velocities for $\chi \in [\pi, 2\pi)$ and a particular orientation angle ϕ will correspond to the appropriately rescaled values obtained for $\chi-\pi$ and $-\phi$. A useful check on the formulation is afforded by ensuring that the velocities

https://doi.org/10.1017/jfm.2013.510 Published online by Cambridge University Press

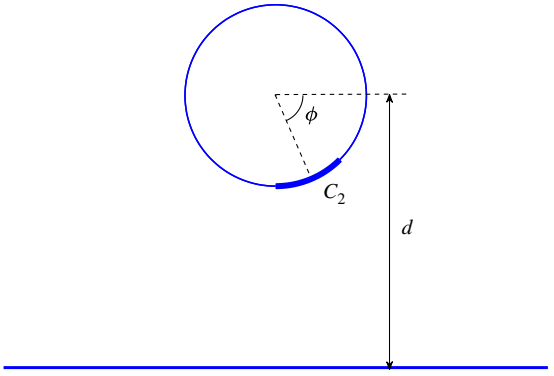


FIGURE 5. (Colour online) Definition sketch for the angle ϕ which is restricted to the interval $\phi \in [-\pi/2, \pi/2]$ so that C_2, shown with a bold line, is directed towards $x > 0$.

obtained, say, for a given ϕ and parameter values $a = -1$, $\chi = \pi/2$ are the same as those obtained for $-\phi$ with $a = -3$, $\chi = 3\pi/2$.

A general rule gleaned from the free-space study is that, if $a < 0$, a particle is expected to move in the direction in which face C_2 points, and this is likely to hold true even in the presence of a wall. A good determinant of the dynamical evolution of a particle can be obtained by studying its angular velocity in different configurations relative to the wall. Figure 6 shows a graph of Ω against orientation ϕ for a Janus particle with $\chi = \pi$ and for different values of d. Clearly $\Omega = 0$ for $\phi = -\pi/2$ and $\phi = \pi/2$ owing to the left–right symmetry of the configurations while, interestingly, $\Omega > 0$ for all intermediate ϕ. Figure 7 shows graphs of U and V as functions of ϕ for $d = 5, 1.75$ and 1.25. A check on the formulation is to verify that the particle velocities tend, in the limit $d \to \infty$, to the free-space values in the absence of a wall; the latter were determined in § 2.1 and, in present notation, are

$$U_{fs} = -\frac{2a}{\chi} \sin\left(\pi - \frac{\chi}{2}\right) \cos\phi, \quad V_{fs} = -\frac{2a}{\chi} \sin\left(\pi - \frac{\chi}{2}\right) \sin\phi. \tag{4.1}$$

Graphs of these quantities are superposed as dashed lines for comparison in figure 7. For $d = 5$ wall effects are weak but become increasingly important as d decreases, as expected. For $\phi = -\pi/2$ and $\phi = \pi/2$ we find $U = 0$, but it is clear that the presence of the wall decreases the particle velocity V either towards or away from the wall. On the other hand, in all other orientations wall interactions serve to increase the particle velocity U along the wall, the effect being largest when $\phi = 0$.

To explore the effects of geometrical asymmetry between the two faces, figure 8 shows graphs of Ω for $\chi = \pi/2$ and $\chi = \pi/10$ for particles at various distances from the wall. In both cases, for most values of d, Ω becomes negative when C_2 faces the wall (i.e. for a range of ϕ values close to $-\pi/2$). Dynamically this might be expected to result in attraction of the particle towards the wall since for $\phi \approx -\pi/2$ face C_2 points towards the wall, resulting in motion towards it, while $\Omega < 0$ will promote this motion by keeping C_2 directed towards the wall. The negativity of Ω ceases to hold, however, once the particle draws sufficiently close to the wall, after which $\Omega \geqslant 0$ for all $\phi \in [-\pi/2, \pi/2]$. Moreover, the critical distance d at which Ω becomes positive for all ϕ is found to decrease with χ. Evidence of this is shown only for $\chi = \pi/2$ and $\chi = \pi/10$ but the same phenomenon is found to hold for all smaller values of χ

https://doi.org/10.1017/jfm.2013.510 Published online by Cambridge University Press

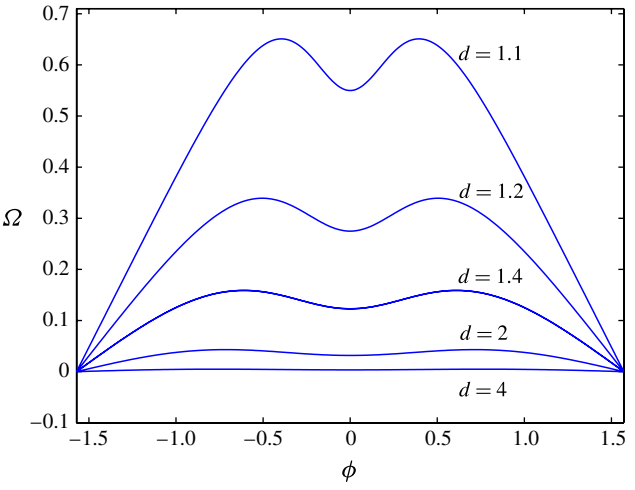


FIGURE 6. (Colour online) Particle angular velocity Ω for $\chi = \pi$ as functions of orientation ϕ for different distances d from the wall.

that we tried. Perhaps the most noteworthy feature of figure 8 is the large range of orientations for which $\Omega > 0$ suggesting that, due to wall interactions, side C_2 will have a tendency to face away from the wall, leading to eventual wall repulsion.

Figures 9 and 10 show graphs of U and V against ϕ for $d = 5, 1.75$ and 1.25 for these two asymmetric particle types. For $\phi \approx -\pi/2$, where C_2 is directed towards the wall, the wall interactions enhance the particle velocity; on the other hand, when C_2 is facing away from the wall the particle velocity is found to decrease from its free-space value. This degree of enhancement, or reduction, of the particle speed increases with proximity to the wall. It is clear that particle orientation is crucial in determining whether wall effects increase or decrease the particle speed. Another interesting feature is that when C_2 is facing away from the wall, and the distance from the wall decreases, V levels out to some positive value, suggesting that the dynamics is determined predominantly by a localized wall interaction region between the portion of face C_1 of the particle which is closest to the wall and depends weakly on the direction of C_2 which is facing away from the near-wall region.

It is easy to carry out full dynamical simulations of the particle motion. The availability of an explicit form (3.53) of the governing dynamical system affords us the opportunity to study the near-wall asymptotics as $Y(t) \to s^+$. From (3.2) this limit can be seen to correspond to $\rho \to 1^-$. It can also be shown from (3.54) that

$$\alpha - \beta = -\frac{\mathrm{i}\rho(1-\rho^2)(\mathrm{e}^{\mathrm{i}\theta} - \mathrm{e}^{\mathrm{i}(\theta+\chi)})}{(1-\mathrm{i}\rho\mathrm{e}^{\mathrm{i}\theta})(1-\mathrm{i}\rho\mathrm{e}^{\mathrm{i}(\theta+\chi)})}, \quad \frac{1}{\alpha} - \frac{1}{\beta} = \frac{\mathrm{i}\rho(1-\rho^2)(\mathrm{e}^{\mathrm{i}\theta} - \mathrm{e}^{\mathrm{i}(\theta+\chi)})}{(\rho^2-\mathrm{i}\rho\mathrm{e}^{\mathrm{i}\theta})(\rho^2-\mathrm{i}\rho\mathrm{e}^{\mathrm{i}(\theta+\chi)})}, \tag{4.2}$$

so both quantities vanish as $\rho \to 1^-$. Hence, inspection of (3.53) reveals that as $\rho \to 1^-$ the dominant terms are

$$\frac{\mathrm{d}X}{\mathrm{d}t} \sim \frac{2a\rho}{\chi(1-\rho^2)} \log\left|\frac{1-\beta}{1-\alpha}\right|, \quad \frac{\mathrm{d}Y}{\mathrm{d}t} \sim \frac{2a\rho}{\chi(1+\rho^2)} \arg\left[\frac{1-\beta}{1-\alpha}\right], \tag{4.3a}$$

$$\frac{\mathrm{d}\theta}{\mathrm{d}t} \sim \frac{2a}{s\chi}\frac{(1+\rho^4)}{(1-\rho^4)} \log\left|\frac{1-\beta}{1-\alpha}\right|. \tag{4.3b}$$

https://doi.org/10.1017/jfm.2013.510 Published online by Cambridge University Press

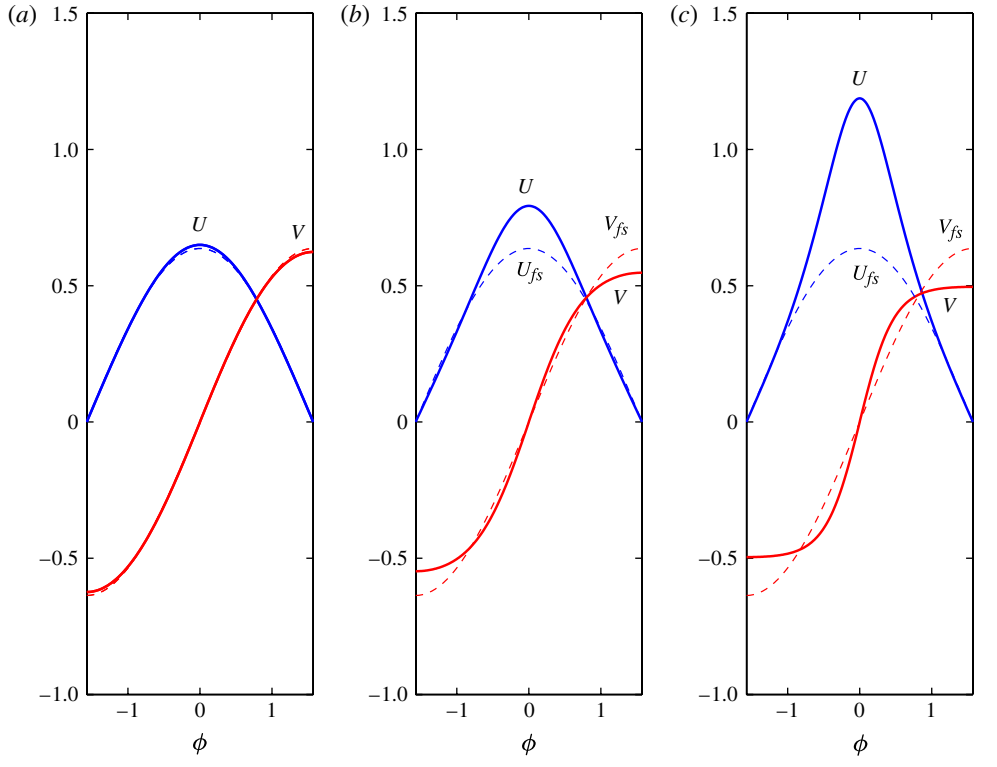


FIGURE 7. (Colour online) Graphs of U and V against orientation angle ϕ for $\chi = \pi$ and distances $d = 5, 1.75$ and 1.25 (a–c). The corresponding free-space velocities U_{fs} and V_{fs} given in (4.1) are superposed as dashed lines. When C_2 faces towards the wall ($\phi = -\pi/2$), or away from it ($\phi = \pi/2$), the particle speed is reduced compared to the free-space value.

The particle velocity perpendicular to the wall therefore tends to a finite non-zero value in this limit, with the angular velocity and the velocity along the wall tending to infinity. We therefore expect two possible dynamical scenarios: either the particle hits the wall in finite time, or it moves away from the wall, possibly drawing close to it first before deflecting from it.

These predictions have been confirmed by numerical simulations. Figure 11 shows $X(t)$, $Y(t)$ and $\theta(t)$ as functions of time for a particle with $s = 1$ and $\chi = \pi$ which hits the wall in finite time. Note that both $X(t)$ and $\theta(t)$ begin to change more rapidly just before touch-down, which is consistent with the near-wall asymptotics just discussed. On the other hand figure 12 shows the evolution for a case where the particle skims the wall, drawing close to it at early times but eventually reorienting face C_2 away from the wall so that the particle moves away. This general behaviour is found to be qualitatively similar for any choice of χ and generic choices of initial conditions. In summary, for any initial distance d from the wall we find there is a range of orientations for which the solute-absorbing face C_2 is directed towards the wall (this range depends on both d and χ), which leads to the particle hitting the wall in finite time. Outside this range, the particle moves away from the wall, even if it first undergoes a short period of initial wall attraction before reorienting and eventually moving away.

https://doi.org/10.1017/jfm.2013.510 Published online by Cambridge University Press

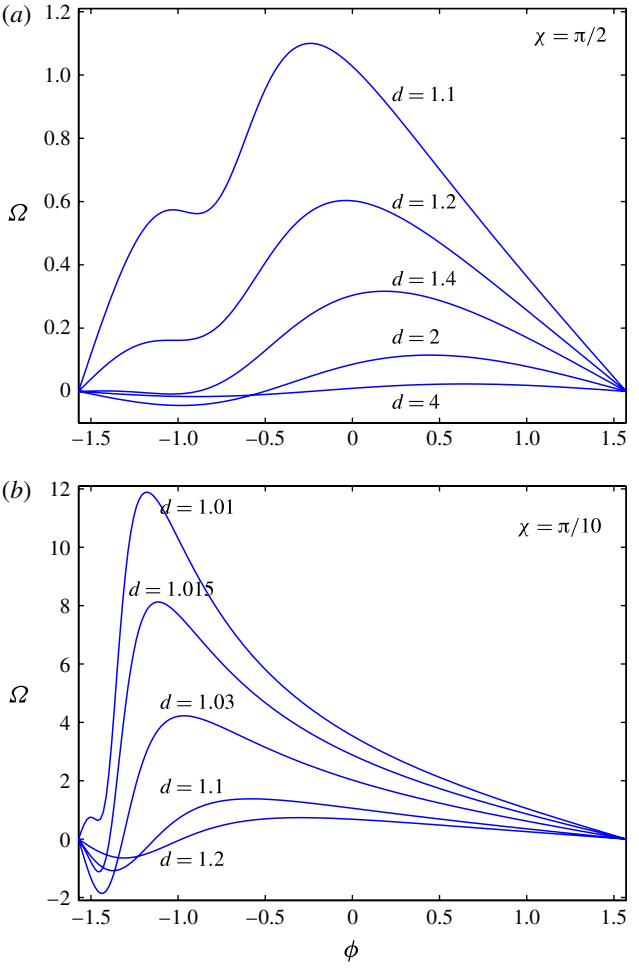


FIGURE 8. (Colour online) Graph of Ω against ϕ for $\chi = \pi/2$ (a) and $\pi/10$ (b) for different distances d from the wall. For any χ a range of ϕ near $-\pi/2$ with $\Omega < 0$ is eventually found to disappear once the particle is sufficiently close to the wall.

We were unable to find any stationary states, steadily translating states, or any nonlinear periodic orbits along the wall as have been observed for low-Reynolds-number treadmilling swimmers (Crowdy & Or 2010; Crowdy & Samson 2010; Crowdy 2011) and for electrophoretic motion of Janus particles near a wall (Gangwal *et al.* 2008; Kilic & Bazant 2011).

5. Discussion

Within a simple physical model, and by deriving an explicit dynamical system governing the motion, this theoretical study has explored the dynamics of two-faced self-diffusiophoretic Janus particles near a plane no-slip wall. For all particles of the special type considered here two dynamical scenarios are found. For a range of initial conditions for which the solute-absorbing face is sufficiently close to the wall and directed towards it we observe that the particle hits the wall in finite time. Outside

https://doi.org/10.1017/jfm.2013.510 Published online by Cambridge University Press

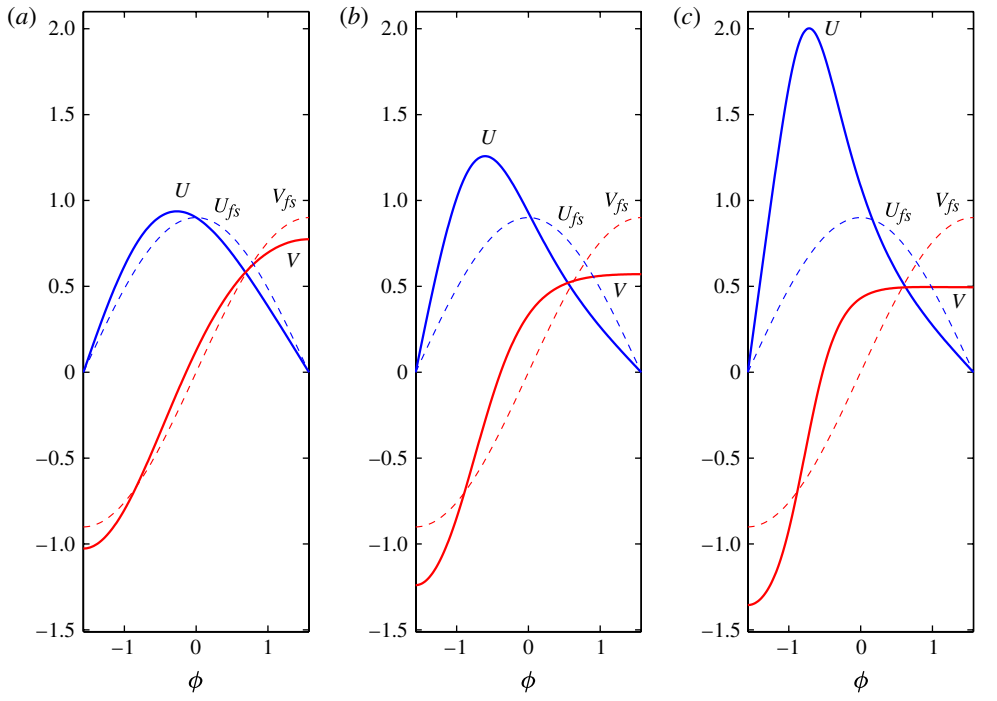


FIGURE 9. (Colour online) Graphs of U and V against orientation angle ϕ for $\chi = \pi/2$ and distances $d = 5, 1.75$ and 1.25 (a–c). The corresponding free-space velocities U_{fs} and V_{fs} given in (4.1) are superposed as dashed lines. When C_2 faces the wall ($\phi = -\pi/2$) the particle velocity is enhanced compared to its free-space value, while it is reduced when C_2 faces away from the wall ($\phi = \pi/2$).

this range of initial conditions we observe the phenomenon of eventual wall repulsion whereby wall interactions serve to reorient the 'nose' of the particle to face away from the wall, leading to the particle being repelled away.

Another observation is that whether the wall increases or decreases, the particle speed depends strongly on both the particle orientation and on the geometry of its faces. For example, a particle with $\chi = \pi$ and face C_2 directed at the wall will travel more slowly towards the wall than it would if the wall was absent, while a particle with $\chi = \pi/2$ in the same orientation will travel faster. These speed enhancement or reduction effects grow stronger with proximity to the wall.

An exhaustive investigation of the parameter space is beyond the scope of the present article, and here we have focused on a particular class of Janus particles with uniform surface mobility and two faces with different surface activity and varying surface coverage. The mathematical approach is adaptable to other scenarios and parameter regimes of interest – e.g. particles that are a net source or sink of solute, ones with faces of differing surface mobilities, multi-faceted or 'Saturn' particles (Golestanian *et al.* 2007), or a chemically active confining wall. It is also adaptable to other situations where the phoretic motion is driven instead by external effects such as electric fields (Keh *et al.* 1991; Zhao & Bau 2007; Kilic & Bazant 2011).

While models involving three-dimensional (e.g. spherical) Janus particles are naturally of greater physical relevance, such investigations will likely have to be performed by means of numerical simulation (as in Kilic & Bazant 2011, for

https://doi.org/10.1017/jfm.2013.510 Published online by Cambridge University Press

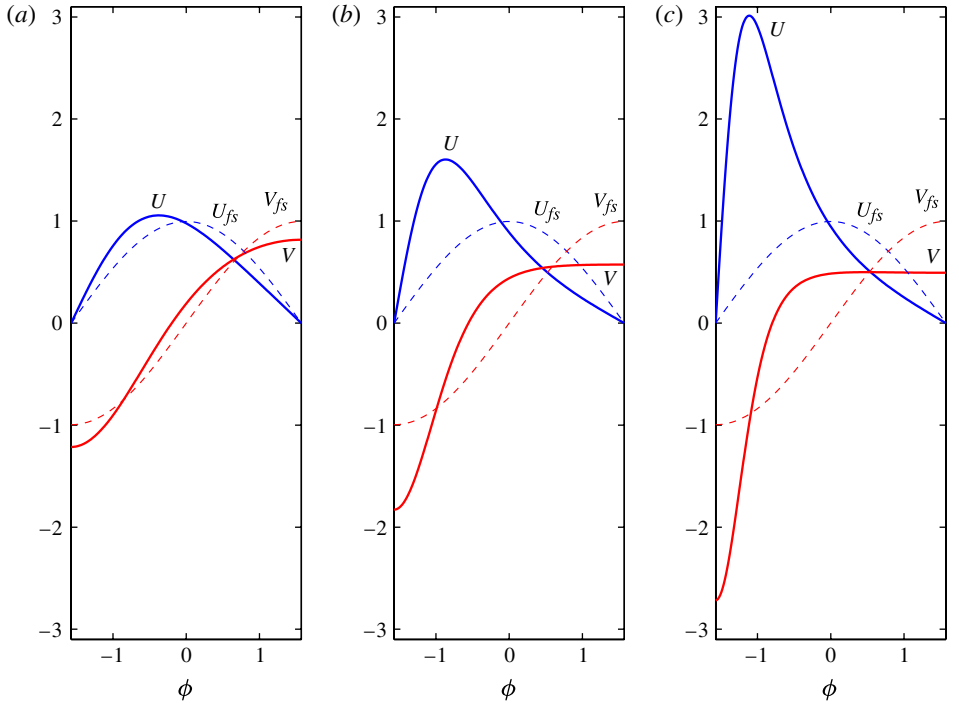


FIGURE 10. (Colour online) Graphs of U and V against orientation angle ϕ for $\chi = \pi/10$ and distances $d = 5$, 1.75 and 1.25 (*a–c*). The corresponding free-space velocities U_{fs} and V_{fs} given in (4.1) are superposed as dashed lines. When C_2 faces the wall ($\phi = -\pi/2$) the particle velocity is enhanced compared to its free-space value, while it is reduced when C_2 faces away from the wall ($\phi = \pi/2$).

example) since any useful analytical progress will be precluded by the complexity of the geometry. Nevertheless the two-dimensional model already provides useful insights as to the possible dynamical behaviours and, given the complexity of the coupled harmonic and biharmonic boundary value problems involved even in the two-dimensional model, it is surely noteworthy and significant that explicit forms (3.53) of the governing nonlinear dynamical systems are available. Our analysis has successfully negotiated, without approximation, the mathematical challenges associated both with the two boundary point singularities on the Janus particle at which the two faces meet, as well as those challenges associated with small particle–wall separations.

Finally we should emphasize the significance of (3.35), which expresses the general result – apparently not previously observed in the literature – that only two of an infinite number of possible modes describing an arbitrary smooth tangential slip profile on the circular boundary – as expressed as an expansion in the special parametric variable ζ – contribute to any particle motion under the conditions that the particle is free of both force and torque. This important general result is likely to be useful in other studies of force and torque-free particle motion in the same geometry.

Acknowledgement

The author acknowledges useful discussions with E. Keaveny and Y. Or and partial financial support from a Leverhulme Trust Research Grant.

https://doi.org/10.1017/jfm.2013.510 Published online by Cambridge University Press

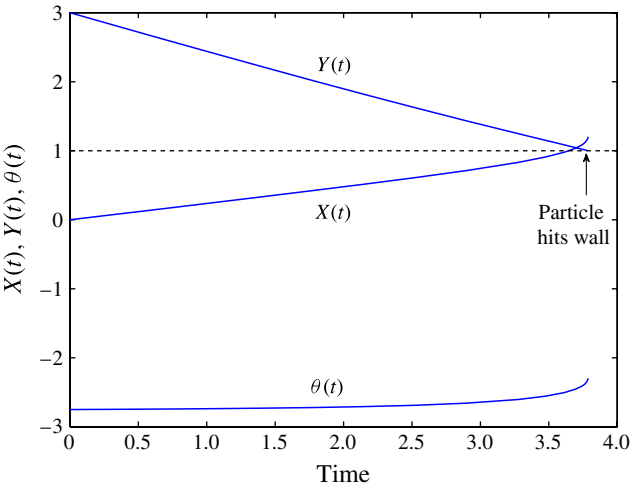


FIGURE 11. (Colour online) Particle hits the wall in finite time: graphs show evolution of $X(t), Y(t)$ and $\theta(t)$ for $\chi = \pi, s = 1$ and initial conditions $Y(0) = 3$, $X(0) = 0$ and $\theta(0) = -3\pi/8 - \chi/2$ (i.e. $\phi(0) = -3\pi/8$).

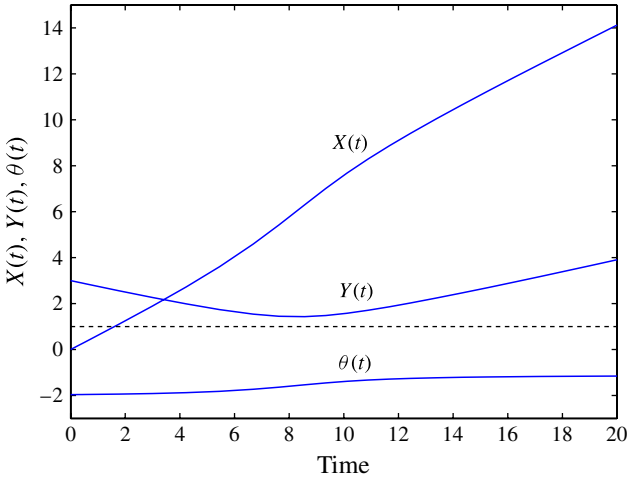


FIGURE 12. (Colour online) Particle skims the wall but moves away: graphs show evolution of $X(t), Y(t)$ and $\theta(t)$ for $\chi = \pi, s = 1$ and initial conditions $Y(0) = 3$, $X(0) = 0$ and $\theta(0) = -\pi/8 - \chi/2$ (i.e. $\phi(0) = -\pi/8$).

Appendix A. Slip velocity calculation

We need to calculate the integral

$$\oint_{|\zeta|=\rho} \frac{\mathrm{d}\mathscr{H}}{\mathrm{d}\zeta} \overline{U}_s^{(s)} \, \mathrm{d}\zeta, \tag{A 1}$$

https://doi.org/10.1017/jfm.2013.510 Published online by Cambridge University Press

where $\mathrm{d}\mathscr{H}/\mathrm{d}\zeta$ is a given rational function of ζ. Now

$$\mathrm{Re}\left[\frac{\mathrm{i}(\zeta-1)(\zeta-\rho^2)}{2R\zeta}\{-G(\zeta)-J(\zeta)\}\right]=\frac{\rho(b-a)}{\pi}\log\left|\frac{\eta(\zeta)}{\eta(1)}\right|. \tag{A 2}$$

Hence

$$\overline{U}_s^{(s)}=\frac{M_j\rho(b-a)}{\pi}\frac{(1-\zeta)}{(\rho^2-\zeta)}\log\left|\frac{\eta(\zeta)}{\eta(1)}\right|,\quad j=1,2. \tag{A 3}$$

The required integrals are therefore

$$\oint_{|\zeta|=\rho}\frac{M_j\rho(b-a)}{\pi}\frac{\mathrm{d}\mathscr{H}}{\mathrm{d}\zeta}\frac{(1-\zeta)}{(\rho^2-\zeta)}\log\left|\frac{\eta(\zeta)}{\eta(1)}\right|\mathrm{d}\zeta. \tag{A 4}$$

Since $\eta(\zeta)$ vanishes at two points α and β on the circle $|\zeta|=\rho$ it is clear that the integrands here have logarithmic singularities on the integration contour. On transferring the integrals to the complex η-plane they assume the form

$$M_1\int_\infty^0 P(\eta)\log\left|\frac{\eta(\zeta)}{\eta(1)}\right|\mathrm{d}\eta+M_2\int_0^{-\infty}P(\eta)\log\left|\frac{\eta(\zeta)}{\eta(1)}\right|\mathrm{d}\eta, \tag{A 5}$$

where

$$P(\eta)=\frac{\rho(b-a)}{\pi}\frac{\mathrm{d}\mathscr{H}(\zeta)}{\mathrm{d}\zeta}\frac{(1-\zeta)}{(\rho^2-\zeta)}\frac{1}{\eta'(\zeta)} \tag{A 6}$$

can be seen to be a rational function of η. Integrals of the form (A 5) can be computed analytically by the results in appendix B.

Appendix B. Residue calculus

The branch of $\log\eta$ has been chosen such that the branch cut is taken along the negative real η-axis with

$$\log\eta=\begin{cases}\log|\eta|+\mathrm{i}\pi & \text{on top of the cut,}\\ \log|\eta|-\mathrm{i}\pi & \text{on the bottom of the cut.}\end{cases} \tag{B 1}$$

Consider the two integrals

$$I_1\equiv\int_\infty^0 P(\eta)\log\left|\frac{\eta(\zeta)}{\eta(1)}\right|\mathrm{d}\eta,\quad I_2\equiv\int_0^{-\infty}P(\eta)\log\left|\frac{\eta(\zeta)}{\eta(1)}\right|\mathrm{d}\eta, \tag{B 2}$$

where $P(\eta)$ is an arbitrary rational function of η assumed to be free of poles on the ray of integration. By means of residue calculus based on the two integration contours in the η-plane shown in figure 13 it can be shown that

$$\begin{aligned}I_1=&-2\pi\mathrm{i}\sum_{upper}\mathrm{Res}\left[P(\eta)\log\eta(\zeta)\right]+\frac{1}{2}\sum_{all}\mathrm{Res}\left[P(\eta)[\log(\eta(\zeta))]^2\right]\\&+\mathrm{i}\pi\sum_{all}\mathrm{Res}\left[P(\eta)\log\eta(\zeta)\right]\\&-\log|\eta(1)|\left[-2\pi\mathrm{i}\sum_{upper}\mathrm{Res}\left[P(\eta)\right]+\sum_{all}\mathrm{Res}\left[P(\eta)\log\eta(\zeta)\right]\right],\end{aligned} \tag{B 3a}$$

$$I_2=-\frac{1}{2}\sum_{all}\mathrm{Res}\left[P(\eta)[\log(\eta(\zeta))]^2\right]+\log|\eta(1)|\sum_{all}\mathrm{Res}\left[P(\eta)\log\eta(\zeta)\right], \tag{B 3b}$$

https://doi.org/10.1017/jfm.2013.510 Published online by Cambridge University Press

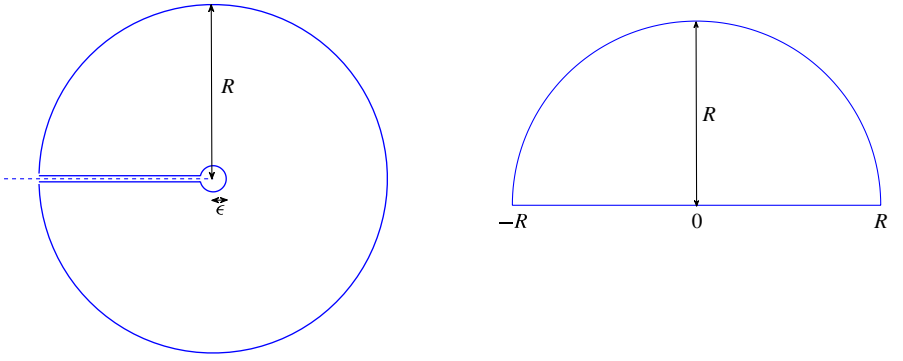


FIGURE 13. (Colour online) The two integration contours in the complex η-plane used to compute I_1 and I_2 in the limit $R \to \infty$ and $\epsilon \to 0$.

where the sum notation is used in an obvious way to denote the sum over all residues in the η-plane or over all residues in the *upper* half-η-plane. To obtain these results the function $P(\eta)\log\eta$ is integrated around both contours while $P(\eta)(\log\eta)^2$ is integrated around the one with the cut along the negative real axis. In the special case where $M_1 = M_2$, as focused on in this paper, the residues of $P(\eta)[\log\eta]^2$ do not contribute, and render the residue calculations more tractable.

REFERENCES

ABLOWITZ, M. & FOKAS, A. S. 1997 *Complex Variables: Introduction and Applications*. Cambridge University Press.

ANDERSON, J. L. 1989 Colloid transport by interfacial forces. *Annu. Rev. Fluid Mech.* **21**, 61–99.

CROWDY, D. G. 2008 The Schwarz problem in multiply connected domains and the Schottky–Klein prime function. *Complex Var. Elliptic Equ.* **53**, 221–236.

CROWDY, D. G. 2011 Treadmilling swimmers near a no-slip wall at low Reynolds number. *Intl J. Non-Linear Mech.* **46**, 577–585.

CROWDY, D. G. & OR, Y. 2010 Two-dimensional point singularity model of a low-Reynolds-number swimmer near a wall. *Phys. Rev.* E **81**, 036313.

CROWDY, D. G. & SAMSON, O. 2010 Hydrodynamic bound states of a low-Reynolds-number swimmer near a gap in a wall. *J. Fluid Mech.* **666**, 721–740.

EBBENS, S. J. & HOWSE, J. R. 2010 In pursuit of propulsion at the nanoscale. *Soft Matt.* **6**, 726–738.

GANGWAL, S., CAYRE, O. J., BAZANT, M. Z. & VELEV, O. D. 2008 Induced-charge electrophoresis of metallodielectric particles. *Phys. Rev. Lett.* **100**, 058302.

GOLESTANIAN, R., LIVERPOOL, T. B. & AJDARI, A. 2005 Propulsion of a molecular machine by asymmetric distribution of reaction products. *Phys. Rev. Lett.* **94**, 220801.

GOLESTANIAN, R., LIVERPOOL, T. B. & AJDARI, A. 2007 Designing phoretic micro- and nano-swimmers. *New J. Phys.* **9**, 126.

JEFFREY, D. J. & ONISHI, Y. 1981 The slow motion of a cylinder next to a plane wall. *Q. J. Mech. Appl. Maths* **34**, 129–137.

KEH, H. J., HORNG, K. D. & KUO, J. 1991 Boundary effects on electrophoresis of colloidal cylinders. *J. Fluid Mech.* **231**, 211–228.

KILIC, M. S. & BAZANT, M. Z. 2011 Induced-charge electrophoresis near an insulating wall. *Electrophoresis* **32**, 614–628.

LAUGA, E. & DAVIS, A. M. J. 2012 Viscous Marangoni propulsion. *J. Fluid Mech.* **705**, 120–133.

MICHELIN, S., LAUGA, E. & BARTOLO, D. 2013 Spontaneous autophoretic motion of isotropic particles. *Phys. Fluids* **25**, 061701.

https://doi.org/10.1017/jfm.2013.510 Published online by Cambridge University Press

MILOH, T. 2013 Dipolophoresis of Janus nanoparticles in a microchannel. *Electrophoresis* **34**, 1939–1949.

PAXTON, W. F., KISTLER, K. C., OLMEDA, C. C., SEN, A., ANGELO, S. K. ST., CAO, Y., MALLOUK, T. E., LAMMERT, P. E. & CRESPI, V. H. 2004 Catalytic nanomotors: autonomous movement of striped nanorods. *J. Am. Chem. Soc.* **126**, 13424–13431.

POPESCU, M. N., DIETRICH, S. & OSHANIN, G. 2009 Confinement effects on diffusiophoretic self-propellers. *J. Chem. Phys.* **130**, 194702.

SQUIRES, T. & BAZANT, M. Z. 2006 Breaking symmetries in induced charge electro-osmosis and electrophoresis. *J. Fluid Mech.* **560**, 65–101.

THUTUPALLI, S., SEEMANN, R. & HERMINGHAUS, S. 2011 Swarming behaviour of simple model squirmers. *New J. Phys.* **13**, 073021.

ZHAO, H. & BAU, H. H. 2007 On the effect of induced electro-osmosis on a cylindrical particle next to a surface. *Langmuir* **23**, 4053–4063.

https://doi.org/10.1017/jfm.2013.510 Published online by Cambridge University Press